Energy 77 (2014) 6–18

Contents lists available at ScienceDirect

Energy

journal homepage: www.elsevier.com/locate/energy

Biomass gasification integrated with a solid oxide fuel cell and Stirling engine

Masoud Rokni

Technical University of Denmark, Department of Mechanical Engineering, Thermal Energy System, Copenhagen, Denmark

ARTICLE INFO

Article history:
Received 24 September 2013
Received in revised form
9 January 2014
Accepted 19 January 2014
Available online 22 February 2014

Keywords:
SOFC
Fuel cell
Hybrid cycle
Stirling engine
Gasification

ABSTRACT

An integrated gasification solid oxide fuel cell (SOFC) and Stirling engine for combined heat and power application is analyzed. The target for electricity production is 120 kW. Woodchips are used as gasification feedstock to produce syngas, which is then used to feed the SOFC stacks for electricity production. Unreacted hydrocarbons remaining after the SOFC are burned in a catalytic burner, and the hot off-gases from the burner are recovered in a Stirling engine for electricity and heat production. Domestic hot water is used as a heat sink for the Stirling engine. A complete balance-of-plant is designed and suggested. Thermodynamic analysis shows that a thermal efficiency of 42.4% based on the lower heating value (LHV) can be achieved if all input parameters are selected conservatively. Different parameter studies are performed to analyze the system behavior under different conditions. The analysis shows that the decreasing number of stacks from a design viewpoint, indicating that plant efficiency decreases but power production remains nearly unchanged. Furthermore, the analysis shows that there is an optimum value for the utilization factor of the SOFC for the suggested plant design with the suggested input parameters. This optimum value is approximately 65%, which is a rather modest value for SOFC. In addition, introducing a methanator increases plant efficiency slightly. If SOFC operating temperature decreases due to new technology then plant efficiency will slightly be increased. Decreasing gasifier temperature, which cannot be controlled, causes the plant efficiency to increase also.

1. Introduction

Due to the ever-increasing demand for more efficient power production and distribution, the main topics of research and development in the field of electricity production are improving efficiency and reducing pollutant emissions, especially that of carbon dioxide. There is currently an increased interest in developing a distributed system of smaller-scale facilities rather than a large-scale facility at a single location, allowing electricity and heat to be produced and distributed close to the end user and thereby minimizing the costs associated with transportation [1,2].

Solid oxide fuel cell (SOFC) stacks will soon enter the commercialization phase, and small Stirling engines are approaching this phase. It therefore would be interesting to integrate these two technologies into a single system, combining the benefits of each system to establish a new technology. Together with an integrated gasification plant that gasifies wood chips in a two-step gasification process, electricity and heat could then be produced in an environmentally friendly way.

SOFCs are one of the most promising types of fuel cells, particularly regarding energy production. They are expected to produce clean electrical energy at high convention rates with low noise and low pollutant emissions [3].

To date, many numerical studies have been performed in order to describe mass and heat transport in SOFC, see e.g. Refs. [4,5], and moreover, studies on syngas from coal and biomass gasification to feed SOFC are carried out, such as [6,7]. Using synthetic wood gas for operating of SOFC is also experimentally studied in Ref. [8] which showed that wood gas from air gasification always gave a stable performance while wood gas from steam gasification did not give clear results. Some missing information from experiments that would be very useful to understand better the operation of SOFCs is briefly presented in Ref. [9].

The exhaust temperatures of SOFCs are high due to the high operating temperature of the cells. Additionally, because the fuel utilization in the fuel cell never reaches 100 percent, the unreacted fuel needs to be combusted in a burner. This combustion in turn produces even hotter off-gases that are perfectly suited for use in a heat engine, such as a Stirling engine, for the production of power and heat for domestic purposes.

E-mail address: MR@mek.dtu.dk.

http://dx.doi.org/10.1016/j.energy.2014.01.078
0360-5442/

Numerous studies have investigated SOFC-based power systems and suggested high thermal efficiencies in the literature. However, the majority of these studies use gas turbines as the bottoming cycle (see, e.g. Refs. [10–12]). A steam turbine has also been used as a bottoming cycle [13,14], resulting in high plant efficiency. Only a few studies have been carried out with a Stirling engine as a bottoming cycle when a fuel cell cycle is used as the topping cycle (see, e.g. Refs. [1,2]). At present, using the Brayton and Rankine cycles as bottoming cycles seems to be the most practical because of the maturity of these technologies. Given that the development trends suggest that the operating temperature of the SOFC will decrease, using gas turbine as bottoming cycle will become less beneficial over time.

Introducing a heat engine (Stirling) as bottoming cycle for SOFC compared to gas turbine and steam cycles has several advantages. Such hybrid cycle is significantly less complex, heat production will be as much as electrical power (high heat-power ratio), small scale CHP (combined heat and power) plants suitable for hotels, hospitals, shopping centers can be built and the plant cost will be much lower.

Integrated gasification SOFC systems have also been studied (see, for example [15–17]). However, there has been an absence of research into integrated biomass gasification SOFC-Stirling CHP plants in the literature, forming the basis of this study.

The present work is an analytical study that conducts a thermodynamic investigation of systems with integrated gasification of woodchips, where the syngas is used as fuel for a SOFC plant that also functions as a topping cycle for a Stirling engine using the heat from the off-gasses exhausted from the topping cycle. The system's net capacity is 120 kW, which is suitable for decentralized CPH plants. The gasifier type used for the analysis is based on the Viking two-stage gasifier built at DTU-Risø. The Viking gasifier plant is a biomass gasifier with an autothermal (air-blown) fixed bed gasifier, which produces a clean syngas that can be directly fed into a SOFC. More information on the gasifier plant can be found in Refs. [18–20]. The SOFC is based on a theoretical model with empirical coefficients calibrated from experimental data. The Stirling engine's parameters are chosen by fitting these parameters to a validated feasible engine.

2. Methodology

The thermodynamic results in this study were obtained using the Dynamic Network Analysis (DNA) simulation tool (see, e.g. Ref. [21]). The software is a result of an ongoing development process at the thermal energy section of the Mechanical Department of the Technical University of Denmark, which began with a Master's thesis project [22]. Since this time, the program has continuously been developed to be generally applicable for different energy systems. The program includes a component library, thermodynamic state models for fluids and standard numerical solvers for differential and algebraic equation systems. The component library content models include heat exchangers, burners, dryers, turbo machinery, decanters, energy storages, valves and controllers, among others. The thermodynamic state models for fluids cover most basic fluids and compounds, such as ash and tar, used in energy system analyses. The calculation procedure is shown in Fig. 1.

DNA is a component-based simulation tool, meaning that the model is formulated by connecting components together with nodes and adding operating conditions to create a system. Next, the physical model will be converted into a set of mathematical equations and solved numerically. The equations will include mass and energy conservation for all components and nodes together with relations for the thermodynamic properties of the fluids in the system. The total mass balance and energy balance for the entire system is also included to account for heat loss and heat exchange between different components. In addition, the components include a number of constitutive equations representing their physical properties, e.g., heat transfer coefficients for heat exchangers and isentropic efficiencies for compressors and turbines. The program is written in FORTRAN, and users may also implement additional components and thermodynamic state models to the libraries.

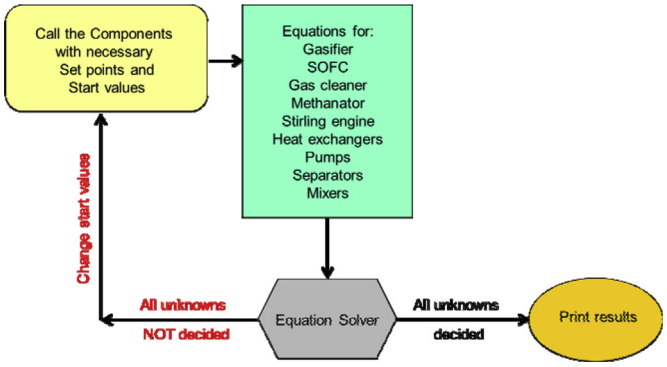

Fig. 1. Calculation procedure.

2.1. Modeling of SOFC stacks

The SOFC model used in this study is based on the planar type developed by DTU-Risø and Topsoe Fuel Cell (TOFC). The model was calibrated against experimental data in the range of 650 °C–800 °C (the average operating temperature), as described in Ref. [23]. For clarification, the model is briefly described below. For this modeling, one must distinguish among electrochemical modeling, the calculation of cell irreversibility (cell voltage efficiency), and the calculation of the species compositions at the outlet. For electrochemical modeling, the operational voltage (E_{cell}) was found to be

$$E_{cell} = E_{Nernst} - \Delta E_{act} - \Delta E_{ohm} - \Delta E_{conc} - \Delta E_{offset} \quad (1)$$

where E_{Nernst}, ΔE_{act}, ΔE_{ohm}, ΔE_{conc} and ΔE_{offset} are the Nernst ideal reversible voltage, activation polarization, ohmic polarization, concentration polarization and offset polarization, respectively. The contribution of the offset polarization is very small; for that reason, it is neglected in this study. Assuming that only hydrogen is electrochemically converted, the Nernst equation can be written as

$$E_{Nernst} = \frac{-\Delta g_f^0}{n_e F} + \frac{RT}{n_e F} \ln\left(\frac{p_{H_2,tot}\sqrt{p_{O_2}}}{p_{H_2O}}\right), \quad (2)$$

$$p_{H2,tot} = p_{H2} + p_{CO} + 4p_{CH4} \quad (3)$$

where Δg_f^0 is the Gibbs free energy (for the H_2 reaction) at standard pressure, F is the Faraday constant, and n_e is the number of electrons transferred in the cell reaction. R and T are the universal gas constant and the operating temperature, respectively. The water–gas shift reaction is very fast; therefore, the assumption that hydrogen is the only species to be electrochemically converted is justified (see Refs. [24,25]). In the above equations, p_{H2} and p_{H2O} are the partial pressures for H_2 and H_2O, respectively.

The activation polarization can be evaluated from the Butler–Volmer equation (see Refs. [26,27]) by isolating it from other polarizations to determine the charge transfer coefficients and the

exchange current density using experimental data and curve fitting. It is modeled as

$$\Delta E_{\mathrm{act}} = \frac{RT}{(0.001698T - 1.254)F}\sinh^{-1}\left[\frac{i_{\mathrm{d}}}{2(13.087T - 1.096\times 10^{4})}\right], \tag{4}$$

where R, T, F and i_{d} are the universal gas constant, operating temperature, Faraday constant and current density, respectively.

The ohmic polarization depends on the electrical conductivity of the electrodes as well as the ionic conductivity of the electrolyte. Again, the model was calibrated against experimental data for a cell with a specified anode thickness, electrolyte thickness and cathode thickness. The model could then be written as (see, e.g. Refs. [28,29])

$$\Delta E_{\mathrm{ohm}} = \left(\frac{t_{\mathrm{an}}}{\sigma_{\mathrm{an}}} + \frac{t_{\mathrm{el}}}{\sigma_{\mathrm{el}}} + \frac{t_{\mathrm{ca}}}{\sigma_{\mathrm{ca}}}\right) i_d, \tag{5}$$

where $t_{\mathrm{an}} = 600$ μm, $t_{\mathrm{el}} = 50$ μm and $t_{\mathrm{ca}} = 10$ μm are the anode thickness, electrolyte thickness and cathode thickness, respectively. σ_{an}, σ_{el} and σ_{ca} are the conductivities of the anode, electrolyte and cathode, respectively.

$$\sigma_{\mathrm{an}} = 10^{5}, \quad \sigma_{\mathrm{ca}} = \frac{5.760\times 10^{7}}{T}\exp\left(-\frac{0.117}{8.617\times 10^{-5}T}\right) \tag{6}$$

$$\sigma_{\mathrm{el}} = 8.588\times 10^{-8}T^{3} - 1.101\times 10^{-4}T^{2} + 0.04679T - 6.54 \tag{7}$$

The concentration polarization is dominant at high current densities for anode-supported SOFCs, wherein insufficient amounts of reactants can be transported to the electrodes and the voltage is then significantly reduced as a direct consequence. The concentration polarization was also calibrated against experimental data by introducing the anode limiting current [30,31] and including the anode properties of porosity and tortuosity. It was then modeled as

$$\Delta E_{\mathrm{conc}} = B\left(-\ln\left(1 + \frac{p_{\mathrm{H2}} i_{\mathrm{d}}}{p_{\mathrm{H2O}} i_{\mathrm{as}}}\right) - \ln\left(1 - \frac{i_{\mathrm{d}}}{i_{\mathrm{as}}}\right)\right), \tag{8}$$

where B is the diffusion coefficient, which was determined using a calibration technique as

$$B = \left(0.008039X_{\mathrm{H2}}^{-1} - 0.007272\right)\frac{T}{T_{\mathrm{ref}}} \tag{9}$$

T_{ref} is the reference temperature (1023 K), and the anode limiting current was defined as

$$i_{\mathrm{as}} = \frac{2Fp_{\mathrm{H2}}D_{\mathrm{bin}}V_{\mathrm{an}}}{RTt_{\mathrm{an}}\tau_{\mathrm{an}}}, \tag{10}$$

where V_{an} and τ_{an} are the porosity and tortuosity of the anode, which are 30% and 2.5 μm, respectively, in the experimental arrangement. The binary diffusion coefficient was given by

$$D_{\mathrm{bin}} = \left(-4.107\times 10^{-5}X_{\mathrm{H2}} + 8.704\times 10^{-5}\right)\left(\frac{T}{T_{\mathrm{ref}}}\right)^{1.75}\frac{p_{\mathrm{ref}}}{p}, \tag{11}$$

which was also calibrated against the experimental data. p_{ref} is the reference pressure, which was 1.013 bar, and X_{H2} is the mass

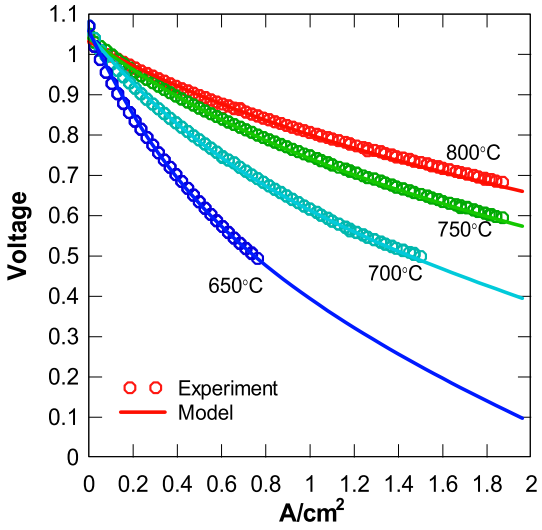

Fig. 2. The cell voltage versus current density and comparison between the model and experimental data with 97% hydrogen and 3% water vapor.

reaction rate of H_2. Lastly, the current density i_{d} is directly proportional to the amount of reacting hydrogen according to Faraday's law:

$$i_{\mathrm{d}} = \frac{\dot{n}_{\mathrm{H2}}2F}{A}, \tag{12}$$

where $\dot{n}_{\mathrm{H2}}$ is the molar reaction rate of H_2. The area A is a physical property of the cell and was 144 cm^2 in this study.

The fuel composition at the anode outlet was calculated using the Gibbs minimization method, as described in Ref. [32]. Equilibria of the anode outlet temperature and pressure were assumed for the H_2, CO, CO_2, H_2O, CH_4 and N_2 species. Thus, the Gibbs minimization method calculates the compositions of these species at the outlet by minimizing their Gibbs energies. Because the methane content in this study is very low, the assumption of equilibrium is reasonable.

To calculate the voltage efficiency of the SOFC cells, the power production from the SOFC (P_{SOFC}) depends on the amount of chemical energy fed to the anode, the reversible efficiency (η_{rev}), the voltage efficiency (η_{v}) and the fuel utilization factor (U_{F}). In mathematical form, it was defined as

$$P_{\mathrm{SOFC}} = \left(\mathrm{LHV}_{\mathrm{H_2}}\dot{n}_{\mathrm{H_2,in}} + \mathrm{LHV}_{\mathrm{CO}}\dot{n}_{\mathrm{CO,in}} + \mathrm{LHV}_{\mathrm{CH_4}}\dot{n}_{\mathrm{CH_4,in}}\right)\eta_{\mathrm{rev}}\eta_{\mathrm{v}}U_{\mathrm{F}}, \tag{13}$$

where U_{F} was a set value and η_{v} was defined as

$$\eta_{\mathrm{v}} = \frac{\Delta E_{\mathrm{cell}}}{E_{\mathrm{Nernst}}} \tag{14}$$

The reversible efficiency is the maximum possible efficiency, defined by the relationship between the maximum electrical energy available (change in Gibbs free energy) and the fuel's LHV (lower heating value), detailed as follows (see Ref. [33]):

$$\eta_{\mathrm{rev}} = \frac{\left(\Delta \bar{g}_{\mathrm{f}}\right)_{\mathrm{fuel}}}{\mathrm{LHV}_{\mathrm{fuel}}} \tag{15}$$

$$\left(\Delta\overline{g}_f\right)_{fuel} = \left[\left(\overline{g}_f\right)_{H_2O} - \left(\overline{g}_f\right)_{H_2} - \frac{1}{2}\left(\overline{g}_f\right)_{O_2}\right] y_{H_2,in} + \left[\left(\overline{g}_f\right)_{CO_2} - \left(\overline{g}_f\right)_{CO} - \frac{1}{2}\left(\overline{g}_f\right)_{O_2}\right] y_{CO,in} + \left[\left(\overline{g}_f\right)_{CO_2} + 2\left(\overline{g}_f\right)_{H_2O} - \left(\overline{g}_f\right)_{CH_4} - 2\left(\overline{g}_f\right)_{O_2}\right] y_{CH_4,in} \quad (16)$$

where $\Delta\overline{g}$ is the average Gibbs free energy from the inlet to outlet and y is the molar fraction. The partial pressures were assumed to be the average between the inlet and outlet:

$$\overline{p}_j = \left(\frac{y_{j,out}+y_{j,in}}{2}\right)\overline{p} \quad j = \{H_2, CO, CH_4, CO_2, H_2O, N_2\}$$
$$\overline{p}_{O_2} = \left(\frac{y_{O_2,out}+y_{O_2,in}}{2}\right)\overline{p}_c \quad (17)$$

Additionally, the equations for conservation of mass (with molar flows), conservation of energy and conservation of momentum were also included in the model.

Comparison between the SOFC model developed here with experimental data is validated in Fig. 2, in terms of current density and cell voltage (IV curve). As can be seen the model capture the experimental data very well at four different cell operating temperatures, varying from 650 to 800 °C. The standard error is less than 0.01. Different hydrogen and water vapor concentrations are used when developing the model. However, here only the data for 97% hydrogen with 3% water vapor concentrations is shown. More details on experiment and calibration procedure can be found in Ref. [23].

2.2. Modeling of the Stirling engine

The Stirling engine is noted for its quiet operation and the ease with which it can use nearly any heat source. Stirling engines are referred to as external combustion heat engines and are operated based on a regenerative closed power cycle using helium, nitrogen, air or hydrogen as the working fluid. An ideal regenerative Stirling cycle consists of four processes in one cycle. First, the working fluid absorbs the heat from a high-temperature reservoir and experiences isothermal expansion (process 1 → 2). Second, the hot working fluid flows through a regenerator, which absorbs heat from the hot working fluid. Thus, the temperature of the working fluid decreases in an isochoric process (2 → 3). Third, the working fluid rejects heat to a low-temperature reservoir and experiences isothermal compression (3 → 4). Lastly, the cold working fluid flows back through the regenerator, which rejects heat to the working fluid. The temperature of the working fluid increases in the second isochoric process (4 → 1).

The model for the Stirling engine used in this study is based on a pseudo Stirling engine described in Ref. [34], providing better agreement to an actual engine than the ideal engine. The main difference between the pseudo Stirling cycle and the ideal Stirling cycle is the assumption of isentropic compression and expansion in the former rather than isothermal compression and expansion in the latter. The detail of the model and its implementation to the in-house program is explained in Ref. [2]. However, for clarification, the model is briefly described here. The model parameter inputs are selected so that construction will be feasible; for example, infinite surface areas of the heat exchangers are not allowed. The heat source used in the analysis is the combustion product gasses from the catalytic gas burner, while water used for domestic purposes is used as the sink. The power output for the Stirling engine are modeled as

$$P_{Stirling} = \eta_{pcy}\left(Q_{high} - Q_{loss}\right) \quad (18)$$

where Q_{loss} is defined as

$$Q_{loss} = Q_{high}\left(1 - \eta_{mec,stirl}\right) \quad (19)$$

where $\eta_{mec,Stirl}$ is the mechanical efficiency of the Stirling engine and Q_{high} is the amount of heat the Stirling engine absorbs from the hot source. The polytrophic efficiency η_{pcy} is defined accordingly as

$$\eta_{pcy} = \left[\frac{\left(1 - RV^{1-\gamma}\right) - \zeta\left(RV^{\gamma-1} - 1\right)}{\left(1 - RV^{1-\gamma}\right) + (1-\zeta)(1-\varepsilon_{stirl})}\right] \quad (20)$$

where RV and ε_{stirl} are the reversibility factor for the Stirling engine and the effectiveness of the internal heat exchangers in the engine, respectively. The constant γ is 1.667, and ζ is defined as the temperature of the cooler gas over the heater gas:

$$\zeta = \left[\frac{T_{cooler,gas} + 273.15}{T_{heater,gas} + 273.15}\right] \quad (21)$$

where $T_{heater\ gas}$ is

$$T_{heater,gas} = T_{heater,wall} - \Delta T_{high} \quad (22)$$

$$T_{cooler,wall} = T_{water,inlet} + 0.66667(\Delta T_{water}) \quad (23)$$

$$T_{cooler,gas} = T_{cooler,wall} + \Delta T_{low} \quad (24)$$

2.3. Modeling of the gasifier

A downscaled version of the Viking two-stage gasifier is modeled and used for the analysis in this investigation. The Viking gasifier is a 75-kW_{th} gasifier built and developed by the Biomass Gasification Group at the Technical University of Denmark [18]. Wood pellets are used as feedstock; the pellets are first dried to remove surface moisture and pyrolysed in the first reactor, after which the pyrolysed products (600 °C) are fed into a downdraft fixed bed char gasifier reactor. The produced exhaust gases are used to heat the reactor for the drying and pyrolysis processes (see Fig. 3). Between pyrolysis and char gasification, the partial oxidation of the pyrolysis products provides the heat for the endothermic char gasification reactions. Char is gasified in the fixed bed, while H_2O and CO_2 are the gasifying agents in the char gasification reactions. The gasifier operates at nearly atmospheric pressure levels.

The gasifier is modeled by implementing a simple Gibbs reactor; thus, when chemical equilibrium is reached, the Gibbs free energy will be at a minimum. This characteristic is used to calculate the gas composition at a specific temperature and pressure without taking the reaction paths into account [32] and will be briefly explained below. The Gibbs free energy of a gas (assuming a mixture of k perfect gases) is

$$\dot{G} = \sum_{i=1}^{k} \dot{n}_i\left[g_i^0 + RT\ln(n_i p)\right] \quad (25)$$

where g^0, R and T are the specific Gibbs free energy, universal gas constant and gas temperature, respectively. Furthermore, each atomic element in the inlet gas is in balance with the outlet gas composition, which shows that the flow of each atom must be conserved. For N elements, this balance is expressed as

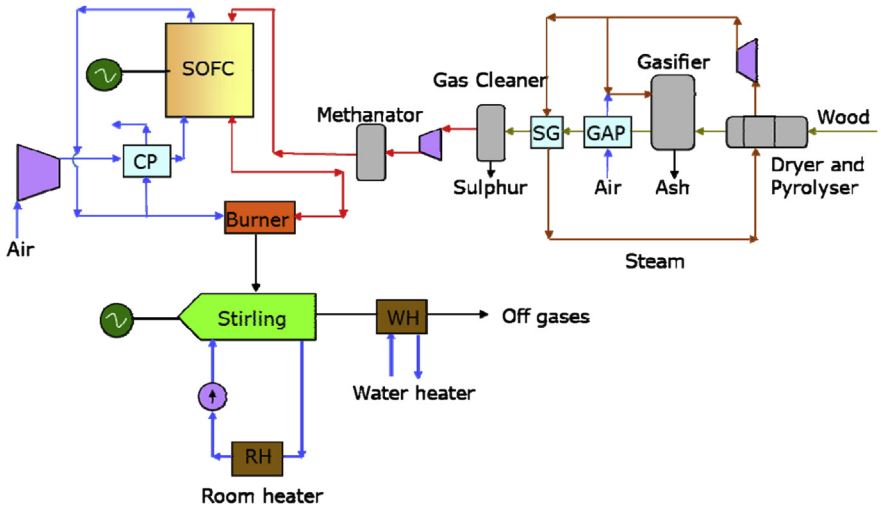

Fig. 3. (a) System layout for the intergraded gasification SOFC-Stirling-based CHP plant.

$$\sum_{i=1}^{k} \dot{n}_{i,\mathrm{in}} \mathbf{A}_{ij} = \sum_{m=1}^{w} \dot{n}_{m,\mathrm{out}} \mathbf{A}_{mj} \quad \text{for } j = 1,\ N \tag{26}$$

where the N elements include H_2, O_2, N_2, CO, NO, CO_2, steam, NH_3, H_2S, SO_2, CH_4, C, NO_2, HCN (hydrogen cyanide), COS (carbonyl sulfide), Ar, and ash (SiO_2) in the gasifying process. $\mathbf{A}_{mj}$ is the number of atoms of element j (H, C, O, N) in each molecule of the entering compound i (H_2, CH_4, CO, CO_2, H_2O, O_2, N_2, and Ar), while $\mathbf{A}_{ij}$ is the number of atoms of element j in each molecule of the exiting compound m (H_2, O_2, N_2, CO, NO, CO_2, steam, NH_3, H_2S, SO_2, CH_4, C, NO_2, HCN (hydrogen cyanide), COS, Ar and ash). The minimization of the Gibbs free energy was achieved by introducing a Lagrange multiplier μ for each of the N constraints obtained in Eq. (26). The expression can then be minimized as

$$\varphi = \dot{G}_{\mathrm{tot,out}} + \sum_{j=1}^{N} \mu_j \left(\sum_{i=1}^{k} \dot{n}_{i,\mathrm{out}} A_{ij} - \sum_{m=1}^{w} \dot{n}_{m,\mathrm{in}} A_{mj} \right) \tag{27}$$

Furthermore, by setting the partial derivative of this equation with respect to $\dot{n}_{i,\mathrm{out}}$ to zero, the function φ can be minimized as

$$\begin{aligned} &\frac{\partial \varphi}{\partial \dot{n}_{i,\mathrm{out}}} = \frac{\partial \dot{G}_{\mathrm{tot,out}}}{\partial \dot{n}_{i,\mathrm{out}}} + \sum_{j=1}^{N} \mu_j A_{ij} = 0 \quad \text{for } i = 1,k \\ &\Rightarrow g^0_{i,\mathrm{out}} + RT \ln\left(n_{i,\mathrm{out}} p_{\mathrm{out}}\right) + \sum_{j=1}^{N} \mu_j A_{ij} = 0 \quad \text{for } i = 1,k \end{aligned} \tag{28}$$

Thus, a set of k equations is defined for each chemical compound leaving the system.

In the previous study, Rokni [17] compared the computed dry wood gas composition with the measured dry wood gas composition from Viking gasifier and showed that the calculated results agreed very well with the measured data.

2.4. Modeling the other components

The compressors' power consumptions are modeled based on the definition of isentropic and mechanical efficiencies ($\eta_{\mathrm{isentropic}}$ and $\eta_{\mathrm{mechanical}}$, respectively) as

$$\eta_{\mathrm{isentropic}} = \left[\frac{W'}{W} = \frac{\Delta h'_0}{\Delta h_0} \right]_{\mathrm{compressor}} \tag{29}$$

$$\eta_{\mathrm{mechanical}} = \left[\frac{\Delta h_0}{\dot{W}} \right]_{\mathrm{compressor}} \tag{30}$$

where the symbol $'$ represents the compression process without isentropic losses and W and h represent work and enthalpy, respectively.

Heat exchangers are all assumed counter flow, and it is assumed that all of the energy is transferred from one side to the other, neglecting heat losses. The logarithmic mean temperature difference (LMTD) and effectiveness-number of transferred units (ε-NTU) methods are used in the calculation of the flows in the heat exchangers, depending on the type [35].

The pumps' power consumption is obtained by volumetric and pressure states as

$$W_{\mathrm{pump}} = \left[\frac{\dot{m} v_{\mathrm{in}} (p_{\mathrm{out}} - p_{\mathrm{in}})}{\eta} \right]_{\mathrm{pump}} \tag{31}$$

where $\dot{m}$, p, v and η are the mass flow, pressure, specific volume (m^3/kg) and efficiency of the pump, respectively.

A methanator increases the content of methane in the fuel by methanation, which is mainly the exothermic reaction of CO and H_2 to reform CH_4 and steam:

$$CO + 3H_2 \rightarrow CH_4 + H_2O \tag{32}$$

However, other minor reactions may also occur depending on the fuel. To model the methanator, a simple Gibbs reactor is also implemented [32,13], meaning that the total Gibbs free energy is minimized when chemical equilibrium is achieved. For the methanator, the species at the outlet are defined as H_2, CO, CO_2, steam, CH_4, N_2, NO, H_2S, SO_2, NO_2, HCN (hydrogen cyanide), COS (carbonyl sulfide), N_2O, NO_3, SO_3 and Ar.

In a catalytic gas burner, the unused fuel is reformed in a highly exothermic process. It is modeled by a general equation for burning the hydrocarbons with oxygen:

$$C_nH_m + \left(n + \frac{m}{4}\right) O_2 \rightarrow nCO_2 + \left(\frac{m}{2}\right) H_2O \tag{33}$$

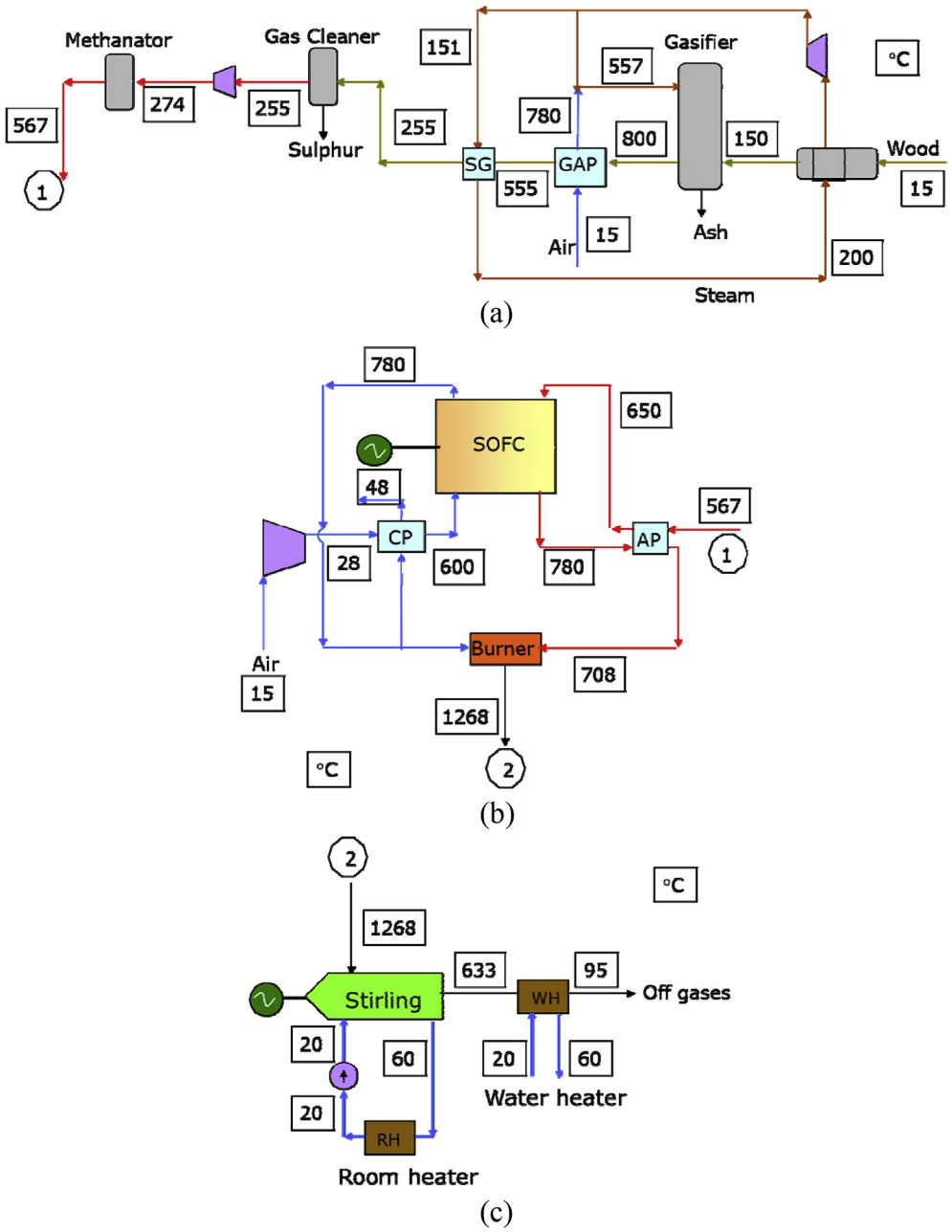

Fig. 4. System layout including temperatures for each stream. (a) Gasification plant including gas cleaner and methanator, (b) SOFC plant, (c) Stirling engine plant including space heating and domestic hot water.

where n and m denote the amount of the hydrocarbon in the reaction. Furthermore, for all reforming processes in any component, the Gibbs free energy is minimized to obtain chemical equilibrium.

The reliability of the components presented here was justified in Ref. [2] by building a benchmark system consisting SOFC, Stirling engine, methanator, heat exchanger, etc., fed with different fuels such as natural gas, ethanol and methanol. The obtained results agreed well with the corresponding results obtained by other researchers in the open literature.

3. Plant configurations

The system investigated here is presented in Fig. 3, which is a small-scale CHP consisting of an integrated biomass gasification plant with an SOFC system functioning as a topping cycle, while a Stirling engine with a water heater comprises the bottoming cycle. Such small scale integrated biomass gasification with SOFC-Stirling with high heat-power ratio is new and has not been investigated previously. Woodchips are fed into a gasifier for the production of syngas via a two-step process. The first step is the drying and pyrolysis of the feedstock, and the second step utilizes a fixed bed gasifier, where the pyrolysed feedstock is gasified by steam and air as gasification agents. Although it was reported in Ref. [20] that the produced syngas is clean enough to be fed directly into the SOFC without additional fuel processing, a gas cleaner is introduced to remove the small contaminants present in the syngas, mainly sulfur. The gas cleaner is assumed to work at a temperature of 250 °C.

Table 1
System operating input parameters.

Parameter	Value
Wood chips temperature	15 °C
Pyrlosis and dry wood temperature	150 °C
Gasifier temperature	800 °C
Gasifier pressure	1 bar
Gasifier pressure drop	0.005 bar
Gasifier carbon conversion factor	1
Gasifier non-equilibrium methane	0.01
Steam blower isentropic efficiency	0.8
Steam blower mechanical efficiency	0.98
Steam temperature in steam loop	150 °C
Wood gas blower isentropic efficiency	0.7
Wood gas blower mechanical efficiency	0.95
Gas cleaner pressure drop	0.0049 bar
Cathode compressor air intake temperature	25 °C
Compressor isentropic efficiency	0.7
Compressor mechanical efficiency	0.95
SOFC operating temperature	780 °C
Anode inlet temperature	650 °C
Cathode inlet temperature	600 °C
Pressure drop, anode side	0.02 bar
Pressure drop, cathode side	0.055 bar
SOFC fuel utilization rate	0.675
Number of cells in stack	74
Number of stacks	160
Heat exchangers pressure drop	0.01 bar
Pinch temperature CP	20 °C
Burner ratio inlet outlet pressure	0.97
Stirling engine heater wall temperature	600 °C
Stirling engine ΔT_{high}	125 °C
Stirling engine ΔT_{low}	60 °C
Stirling engine compression ratio	1.44
Heat exchanger efficiency, Stirling engine	0.98
Stirling engine loss factor	0.8
Stirling engine heat sink inlet temperature	20 °C
Stirling engine heat sink outlet temperature	60 °C
Water pump efficiency	0.95
Inlet water temperature water heater	20 °C
Outlet water temperature water heater	60 °C
Off gas temperature (after water heater)	95 °C

For the topping SOFC cycle, the ambient air at 15 °C is compressed to the working pressure of the SOFC (normal pressure) and then heated in the cathode air preheater (CP) to 600 °C before entering the cathode side of the SOFC stacks. Fig. 4 displays the temperatures of each stream, divided in gasification plant including gas cleaner as well as methanator (Fig. 4a), SOFC plant (Fig. 4b) and Stirling engine plant with domestic hot water production (Fig. 4c). The cathode preheater uses some of the SOFC off-air to heat the incoming air. The off-air is split into two streams: one entering the CP and the other entering the catalytic burner (CB). For the anode side, the cleaned syngas is first pumped to compensate for the pressure drop along the way. Next, the syngas is reformed exothermically in a methanator, wherein the CH_4 content in the gas is increased from a molar fraction of approximately 0.01 to nearly 0.05. This increase is at the expense of the molar fractions of H_2, CO, and steam, while those of N_2 and CO_2 have increased. This change will not affect the SOFC's electrical production in any particular way; however, because the reformation is highly exothermic, less heat needs to be extracted from the SOFC off-fuel to heat the incoming fuel to the SOFC fuel inlet temperature of 650 °C through the anode preheater (AP). This will eventually provide the Stirling engine with a larger amount of heat to be used because the fuel will be at a higher temperature when entering the CB, and the combustion processes will therefore occur at a higher temperature. The CB is implemented because not all of the fuel is reacted in the SOFC stacks due to fuel utilization. The entering temperatures mentioned above are essential requirements for the proper functioning of SOFC stacks, not only to initiate the chemical reactions but also to avoid cell thermal fractures.

Secondly, the use of a larger molar fraction of CH_4 in the SOFC causes endothermic internal reforming, reducing the amount of air used for cooling purposes and maintaining the SOFC operating temperature at 780 °C. Thus, the workload of the cathode compressor/air blower will decrease.

For the bottoming cycle, a Stirling engine is implemented. The Stirling engine utilizes the combustion products, leaving the CB as a heat source. The water used as the heat sink enters at 20 °C and exits at 60 °C, making it appropriate for, e.g., domestic hot water for heating. In particular, its temperature is sufficient to address problems related to bacteria, e.g., Legionella [36], and for use in domestic applications. The heat remaining after the Stirling engine is used for domestic hot water. Water is constrained in the same manner as the heat sink, and the combustion products leave the system into the environment at approximately 95 °C, which is hot enough to avoid corrosion problems.

4. Results and discussion

The gasification plant integrated with SOFC-Stirling presented here is new and has not been investigated previously in the open literature. Also, introducing a methanator after the gasifier is new and has not been discussed previously for such plants. Thus, the current study can be regarded as a continuation study carried out in Ref. [2]. The main operating parameters for the plant are presented in Table 1. Ambient conditions are assumed to be 1 bar and 15 °C.

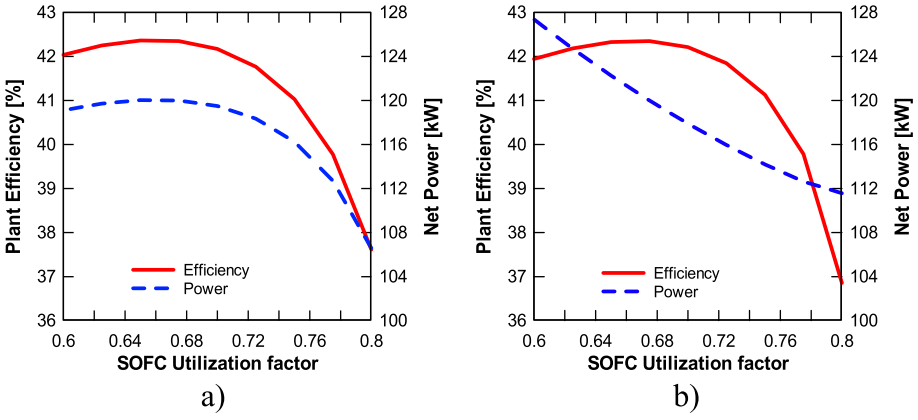

Fig. 5. Plant thermal efficiency and net power production as a function of woodchip mass: a) constant woodchip mass flow and b) constant SOFC electrical power.

Table 2
Molar fraction composition of wood and syngas.

Compound/molar fraction	Wood	Syngas	Methanated syngas	Off-gases
Hydrogen	0.041	0.253	0.220	
Nitrogen	0.001	0.288	0.310	0.5303
Carbon monoxide		0.172	0.086	
Carbon dioxide		0.116	0.186	0.173
Water (liquid)	0.332			
Water (gas)		0.158	0.147	0.255
H_2S ($\times 10^5$)		4.571	–	
Methane		0.010	0.049	
Argon		0.003	0.004	0.004
Oxygen	0.293			0.038
Carbon	0.326			
Sulfur ($\times 10^4$)	1.336			
Ashes	0.006			

Each SOFC stack is assumed to contain 74 cells, and the number of stacks is chosen as 160, although other values could be used. However, the plant cost increases in proportion with the number of stacks. Thus, the number of stacks must be selected based on cost estimation calculations, which is beyond the scope of this study. Although not shown here, a simple cost estimation revealed that choosing 150–160 stacks would be reasonable in terms of plant cost. The operating temperature of the gasifier is 800 °C, while the operating temperature of the SOFC cells is selected to be 780 °C. The SOFC current density and cell voltage are calculated as 0.806 A/cm^2 and 0.720 V, respectively.

To achieve a 120-kW output of electrical energy, the gasifier needs a fuel input of approximately 88.48 kg/h, leading to a syngas production of approximately 176.4 kg/h. Therefore, this amount of biomass should be provided to the unit from either the available biomass from agriculture or a cultivation area.

Another important parameter to be chosen is the utilization factor of the SOFC cells. To select this parameter, two different sets of calculations are carried out for the parameters given in Table 1: one in which the feedstock mass flow is kept constant, and one in which the electrical power produced by the SOFC stacks is kept constant. The results are displayed in Fig. 5, which shows that the plant efficiency will be highest at a certain utilization factor. This value is found to be approximately 0.65 and 0.675 for the cases of constant feedstock mass flow and constant electrical power, respectively. Thus, the value 0.675 is used here for all further calculations unless another value is mentioned.

The syngas molar fraction and the off-gas composition are presented in Table 2. Because ambient air is used as one of the gasifying agents, a large portion of unusable N_2 is present in the syngas. The syngas consists of a small portion of H_2S (ppm level), which can easily be removed in a desulphurization unit. Some steam is also present in the syngas because the small-scale gasifier used here cannot completely dry up the produced gas. This facilitates the application of a methanator prior to SOFC without using anode recirculation or external steam supplement. This feature also leads to a larger mass flows, which are beneficial for Stirling engine operation. In the methanator, the amount of methane is increased by reacting steam and carbon monoxide as the main reactants. The molar faction of methane is increased by a factor of approximately five.

For SOFC, however, a large amount of N_2 and steam causes concentration polarization at a rather early stage. The SOFC has a power output of 98.8 kW, whereas the Stirling engine provides 26.9 kW of power (see Table 3). The internal power consumption is 5.8 kW, which is mainly due to the cathode air compressor. The high power consumption of the cathode air compressor is because this compressor also provides the cooling effect needed to maintain the SOFC temperature at the desired level. The reaction inside the SOFC is highly endothermic; therefore, it needs a relatively high air flow to cool the cells.

The thermal efficiency of the topping SOFC cycle is 0.329 LVH, which is somewhat low for a SOFC system. However, the entire plant has a thermal efficiency of 0.424 LVH, which is a respectable value for such a small-scale system. The implementation of the bottoming Stirling engine gives a remarkable increase in plant efficiency of 28.9 percent. It is found that the Stirling engine's heat sink produces nearly two-thirds of the domestic water heating. The two water heaters together produce 127.33 kW.

It is also assumed that the plants' internal electrical consumption is covered by its production, meaning that the net electricity production of 120 kW is

$$P_{\text{net}} = P_{\text{SOFC}} + P_{\text{Stirling}} - \sum_n P_{\text{el},n,\text{consumed}} \tag{34}$$

where P_{SOFC} and P_{Stirling} are the power production from the SOFC and Stirling engine, respectively, and $P_{\text{el},n,\text{consumed}}$ is the consumption of power from the n-th component. The thermal efficiency of the plant is calculated by the net power production of the SOFC and Stirling engine compared to the fuel input:

$$\eta_{\text{th,plant}} = \left[\frac{P_{\text{net}}}{\dot{m}_{\text{fuel}} \times \text{LHV}_{\text{fuel}}}\right] \tag{35}$$

Introducing a methanator for syngas and study its effect on plant performance is not investigated preciously and it would be interesting to see how plant efficiency is affected by increasing the methane content in the syngas. The effect of the methanator on the plant performance is shown in Table 4. As seen, the plant efficiency is increased by approximately 2% when a methanator is included. The hydrogen concentration is slightly reduced after the methanator; therefore, the power produced by the SOFC also decreases. On the other hand, increasing the methane content encourages less heat to be produced inside the SOFC, thereby decreasing the cooling air flow. It can be seen that the power consumption is considerably decreased when the methanator is included; thus, the plant

Table 3
Plant output for the initial operating parameters.

Parameter	System output
Feedstock consumption	88.48 kg/h
Produced amount of syngas	176.4 kg/h
Electric power output, SOFC stacks	98.90 kW
Power output, Stirling engine	26.91 kW
Total power consumption	5.814 kW
Thermal efficiency, SOFC cycle	0.329
Thermal efficiency of plant	0.424
Percentage increase when adding Stirling cycle	28.9%
Component	**Produced heat [kW]**
Stirling engine	53.5
Water heater	73.83
Total hot water production	127.33
Fuel utilization (CHP efficiency)	89.33%

Table 4
Effect of the methanator on plant performance with 84.49 kg/h of woodchips.

Parameter	Without methanator	With methanator
Plant electrical efficiency, (%)	40.29	42.35
Net power production, (kW)	114.2	120.0
Power consumption, (kW)	7.353	5.814
SOFC electric power, (kW)	99.07	98.90
Stirling engine electric power, (kW)	22.45	26.91

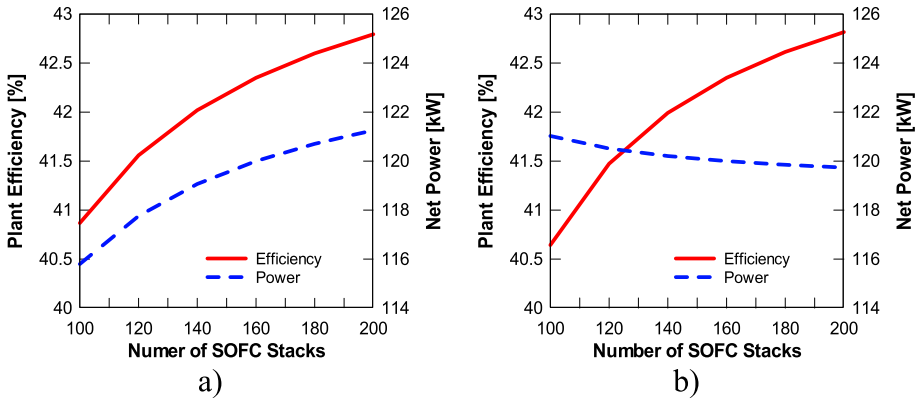

Fig. 6. Plant thermal efficiency and net power production as a function of number of SOFC stacks: a) constant woodchip mass flow and b) constant SOFC electrical power.

efficiency is increased even though less power is produced by the SOFC cells.

5. Parameter investigation

The most important parameters to investigate are the woodchip mass flow, number of SOFC stacks and SOFC utilization factor. The woodchip mass flow indicates the cultivation area to be allocated to provide the required fuel mass flow. The number of SOFC stacks is directly related to the SOFC purchase cost and thereby the investment cost, while the utilization factor affects the amount of off-fuel (fuel remaining after the SOFC stacks) available for the bottoming cycle (Stirling engine in this case). Lowering the utilization factor provides more fuel for the Stirling engine, allowing it to produce more power. That is, the utilization factor affects the cooperation between the two cycles: the SOFC plant and the Stirling engine.

Other parameters of interest are the SOFC and gasifier average operating temperatures. The SOFC average operating temperature is specified by the manufacturer and can be controlled by the oven, while the gasifier average temperature cannot be controlled and varies between 750 °C and 850 °C.

5.1. Number of SOFC stacks

Following the discussions above, the first parameter investigated was the number of SOFC stacks. Again, to study the effect of the number of SOFC stacks on plant performance, the mass flow of woodchips can be kept constant while the electrical power produced by the SOFC plant is allowed to vary or vice versa. The results are shown in Fig. 6.

For the case with constant fuel flow, both plant efficiency and net power are increased when the number of stacks increases. The power generation in the SOFC stacks is greater when more stacks are used, which in turn increases plant efficiency and net power production (see Fig. 7a). Although the power production by the Stirling engine decreases slightly, the increase in the SOFC power generation rate dominates. However, when the power produced by the SOFC is kept constant but the number of stacks is increased, the fuel mass flow decreases. Decreasing the woodchip mass flow directly affects the power produced by the Stirling engine. However, the rate at which the power produced by the Stirling engine decreases dominates the rate of fuel mass flow reduction. As a result, the net power is lowered (see Fig. 7b).

5.2. Gasifier operating temperature

Another parameter that affects the plant performance is the gasifier operating temperature. However, the gasifier temperature cannot be controlled and varies between 750 °C and 850 °C.

To study the effect of the gasifier operating temperature, the gas composition as function of gasifier temperature must also be studied. Thus, simulations are conducted to study the effect of gasifier operating temperature on plant performance, and the results are shown in Fig. 8. Keeping the fuel mass flow constant and

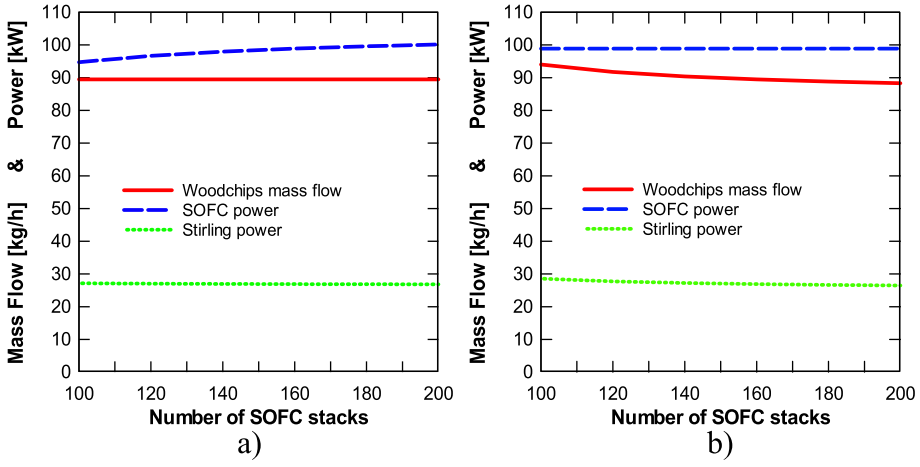

Fig. 7. Power generation as a function of number of SOFC stacks for constant fuel mass flow: a) constant fuel mass flow and b) constant SOFC power.

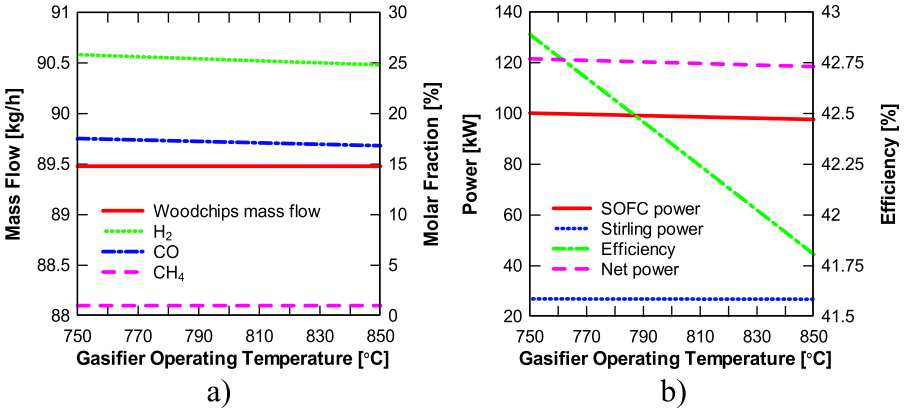

Fig. 8. Plant performance with constant woodchip mass flow: a) syngas molar fraction and b) plant efficiency and power.

decreasing the gasifier operating temperature, the plant efficiency also decreases slightly because the decrease in the gasifier temperature slightly decreases the molar fraction of H_2, while the amount of CH_4 and CO remains essentially the same (see Fig. 8a). The H_2 molar fraction decreases from 25.8% at 750 °C to 24.8% at 850 °C. Although this change is not very large, the plant efficiency is decreases from 42.9% to 41.8%. The plant net power also decreases from 121.5 kW to 118.5 kW within this temperature range. The power from the Stirling engine remains nearly constant. Nevertheless, these changes are small and may be neglected within the temperature range of the gasifier.

It is also possible to allow the fuel mass flow to be varied while the SOFC electrical power is kept constant when the operating temperature of the gasifier is changed within the temperature interval mentioned above (750 °C–850 °C). The calculated results are shown in Fig. 9 for this case. The H_2 molar fraction is decreased slightly, and the fuel mass flow is increased to keep the SOFC electrical power constant. Because the Stirling engine power does not change significantly, the net power from the plant does not change either. The plant efficiency decreases due to the increased fuel mass flow and the definition of thermal efficiency (c.f. Eq. (35)).

5.3. Average operating temperature of SOFC

Another important parameter to investigate is the operating temperature of the SOFCs. In the current study, it was assumed that the cells are operating at 780 °C, although other values could be chosen. The operating temperature of the SOFCs varies from 750 °C to 850 °C depending on the electrotype and manufacturer. Some manufactures are allowing low-temperature operating temperatures, such as 650 °C, in their next generation of products. Therefore, the operating temperature of the cells is allowed to vary from 650 °C to 850 °C. As mentioned above, the inlet temperature of the cells is assumed to be lower than the average operating cell temperature, which in this study is assumed to be 130 °C for the anode side and 180 °C for the cathode side. For planar SOFC types, an overly small difference between the inlet temperature and the average cell operating temperature may lead to cell fatigue, which permanently damages the cells. It is therefore reasonable to decrease the inlet temperature at the same rate as the average cell temperature. This is the case assumed in this investigation. The outlet temperatures of the cells are assumed to have the same values as the average cell operating temperature. Thus, two cases are simulated, one with constant woodchip mass flow (variable SOFC electric power) and one with constant SOFC electrical power (variable fuel mass flow). The results are shown in Fig. 10.

Increasing the average cell operating temperature while keeping the fuel mass flow constant decreases the power from the SOFC stacks. Consequently, the net power and plant efficiency are also decreased. When the SOFC operating temperature is increased, more heat will be fed to the Stirling engine. This increase in energy for the bottoming cycle directly increases the power production (see Fig. 10a). However, the decrease in power dominates over the increase in power for the Stirling engine.

Increasing the average SOFC operating temperature while keeping its electrical power constant can only be achieved when the fuel supplied to the SOFC is also increased. Because the power increase from the Stirling engine is small, the plant net power

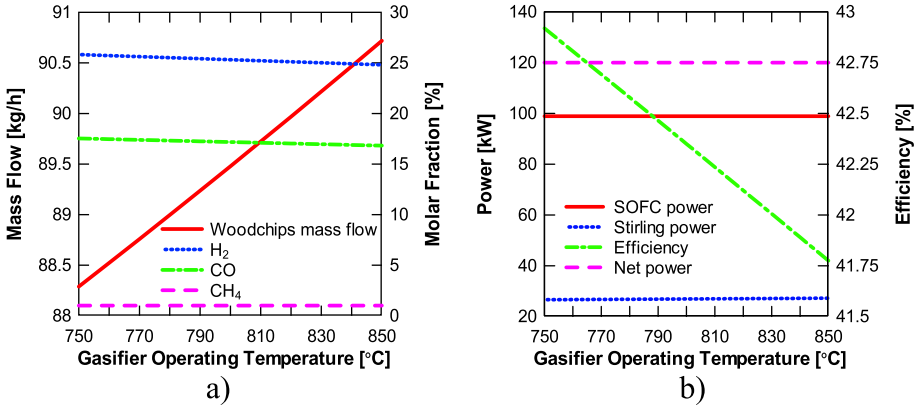

Fig. 9. Plant performance with variable woodchip mass flow (constant SOFC power): a) syngas molar fraction and b) plant efficiency and power.

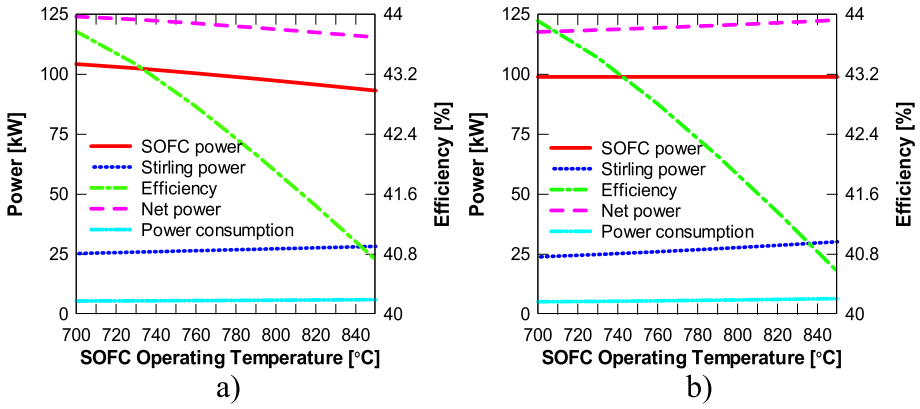

Fig. 10. Plant performance with a) constant woodchips and b) constant SOFC electrical power.

production is also increased slightly. Due to the efficiency definition (Eq. (34)) and increase in fuel mass flow, the plant efficiency is lowered as a direct result (see Fig. 10b). This result is very interesting because it means that lowering the SOFC average operating temperature is favorable for this integrated gasification SOFC-Stirling engine (IGSSE) hybrid plant. At 700 °C, the plant efficiency for fixed feedstock and fixed SOFC electrical power is 43.77%, compared to 43.91%.

As can be seen in Fig. 10, the results for an operating temperature of 650 °C are not shown. This omission is due to the finding that further lowering the average temperature of the SOFC to this temperature prevents the AP (anode preheater in Fig. 3) from acting as a preheater because the heat from the anode outlet is not sufficient to preheat the fuel in the anode side. Therefore, at this low operating temperature, the anode preheater must be removed from the system. The results for the average cell operating temperature of 650 °C without the AP are shown separately in Table 5. A plant efficiency of approximately 43.4% is obtained for both cased with woodchip mass flows of approximately 88.5 and 88.6 kg/h for fixed feedstock respective fixed SOFC electric power. The plant efficiency for a cell temperature of 650 °C is slightly lower than the case of a temperature of 700 °C (c.f. Fig. 10). The cause of this difference is that the fuel fed to the anode is assumed to be 130 °C lower than the operating cell temperature. This temperature difference has a small effect on cooling the SOFC stacks to the desired operating temperature. For the case of an operating temperature of 650 °C, the fuel is fed at 565 °C (see table), which is only 85 °C lower than the cell operating temperature. Thus, the cooling effect from the fuel is decreased, and the air mass flow must be slightly increased to compensate for this loss. Consequently, the power consumption will slightly be increased relative to the case for which the methanator temperature was 130 °C lower than the anode inlet temperature. Removing the methanator has a much worse effect, as discussed above.

Table 5
Plant performance when the AP is removed and the average SOFC temperature is 650 °C.

Parameter	Fixed feedstock	Fixed SOFC power
Plant electrical efficiency, (%)	43.36	43.39
Net power production, (kW)	122.9	121.8
Power consumption, (kW)	5.526	5.469
SOFC electric power, (kW)	104.9	104.1
Stirling engine electric power, (kW)	23.44	23.22
Methanator temperature, (°C)	565.1	565.1
Fuel mass flow, (kg/h)	88.48	88.66

5.4. Comparison with similar studies

Although there exist a few studies on combined SOFC–Stirling system without gasification ([37–42]) but none of these studies present a detailed balance of plant configuration and therefore it would be difficult to compare the results obtained here with these studies. In addition, all of these studies use pure hydrogen as fuel. In these studies the SOFC acts as a hot reservoir source for the irreversible heat engine, neglecting practical irreversibility of heat transfer and other irreversibility effects. It seems that Ref. [2] is the only study that presents a detailed plant configuration consisting of SOFC and heat engine (but without gasification) in the open literature [2] obtained a plant efficiency of about 58–62% depending on the type of the fuel. Thus introducing biomass gasification to the combined SOFC–Stirling hybrid systems decreases plant efficiency by more than 16 points percent. This is aligned with other combined cycles when a gasifier is integrated to the plant. Such drop in electrical efficiency is not only the effect of integrated gasification but also depends on the nature of syngas obtained from fuel (biomass is this case) together with the type of gasifier. Thus, it would be interesting to study the effect of other gasification processes such as coal gasification, waste gasification, etc. on plant efficiency of such hybrid systems.

6. Conclusion

A small-scale integrated gasification SOFC-Stirling CHP plant with a net capacity of 120 kW is presented and thermodynamically investigated. The major conclusions and founding are as follows:

- Plant efficiency of more 42% is possible to achieve for an electrical power of 120 kW which is relatively high when compared with existing large scale integrated gasification plants.
- The plant produces a total heat production of 127 kW in terms of space heating and domestic heat water.
- Introducing a methanator increases plant electrical efficiency from about 40% to about 42%.
- Adding a Stirling engine as bottoming cycle for the SOFC plant increases plant electrical efficiency about 29%.
- There exists an SOFC utilization factor for which the plant efficiency is maximized. This value depends on the number of SOFC stacks.
- The variation of the gasification operating temperature slightly affects plant efficiency and power. When the gasifier temperature increases, the plant efficiency decreases.

- Decreasing the operating temperature of the SOFCs is favorable for such hybrid plants in terms of plant efficiency. The plant efficiency increases as the cell operating temperature decreases until 700 °C or 650 °C. These temperature levels are representative of the development of future SOFC generations.

Acknowledgment

The authors would like to thank the ForskEL-programme of Energinet.dk for financial support of this research through BioSOFC project. Energinet.dk had no influence on the research presented in this article or the writing of the article.

References

[1] Sanchez D, Chacartegui R, Torres M, Sanchez T. Stirling based fuel cell hybrid systems: an alternative for molten carbonate fuel cells. Power Sources 2008;192:84–93.
[2] Rokni M. Thermodynamic analysis of SOFC (solid oxide fuel cell) – Stirling hybrid plants using alternative fuels. Energy 2013;61:87–97.
[3] Calise F, Dentice d'Accadia M, Palombo A, Vanoli L. Simulation and exergy analysis of a hybrid solid oxide fuel cell (SOFC)–Gas turbine system. Energy 2006;31:3278–99.
[4] Arpino F, Massarotti N. Numerical simulation of mass and energy transport phenomena in solid oxide fuel cells. Energy 2009;34(12):2033–41.
[5] Iwai H, Yamamoto Y, Saito M, Yoshida H. Numerical simulation of intermediate-temperature direct-internal-reforming planar solid oxide fuel cell. Energy 2011;36(4):2225–34.
[6] Doherty W, Reynolds A, Kennedy D. Computer simulation of a biomass gasification-solid oxide fuel cell power system using Aspen Plus. Energy 2010;35(12):4545–55.
[7] Ghosh S, De S. Energy analysis of a cogeneration plant using coal gasification and solid oxide fuel cell. Energy 2006;31(2–3):345–63.
[8] Buchinger G, Hinterreiter P, Raab T, Griesser S, Lawlor V, Klein K, et al. Stability of micro tubular SOFCs operated with synthetic wood gases and wood gas components. IEEE; 2007. pp. 444–9. 1-4244-0632-3/07.
[9] Lawlor V. Highlighting of critical experimental data for SOFC modeling that is missing from the literature and potential of N-IR thermography for SOFC study. Fuel Cell Sci Technol 2012;9(024501):1–4.
[10] EG&G and G Technical Services Inc. Fuel cell handbook. Edition 7. U.S. Departement of Energy, Office of Fossil Energy, National Energy Technology Laboratory; 2004.
[11] Riensche E, Achenbach E, Froning D, Haines MR, Heidug WK, Lokurlu A, et al. Clean combined-cycle SOFC power plant-cell modeling and process analysis. Power Sources 2000;86(1–2):404–10.
[12] Pålsson J, Selimovic A, Sjunnesson L. Combined solid oxide fuel cell and gas turbine systems for efficient power and heat generation. Power Sources 2000;86(1):442–8.
[13] Rokni M. Thermodynamic analysis of an integrated solid oxide fuel cell cycle with a Rankine cycle. Energy Convers Manag 2010;51(12):2724–32.
[14] Rokni M. Plant characteristics of an integrated solid oxide fuel cell and a steam cycle. Energy 2010;35:4691–9.
[15] Proell T, Aichering C, Rauch R, Hofbauer H. Coupling of biomass steam gasification and SOFC-gas turbine hybrid system for highly efficient electricity generation. In: ASME turbo Expo proceeding; 2004. pp. 103–12. GT2004-53900.
[16] Bang-Møller C, Rokni M. Thermodynamic performance study on biomass gasification, solid oxide fuel cell and micro gas turbine hybrid systems. Energy Convers Manag 2010;51:2330–9.
[17] Rokni M. Thermodynamic investigation of an integrated gasification plant with solid oxide fuel cell and steam cycles. Green 2012;2:71–86.
[18] Henriksen U, Ahrenfeldt J, Jensen TK, Gøbel B, Bentzen JD, Hindsgaul C, et al. The design, construction and operation of a 75 kW two-stage gasifier. Energy 2006;31(10–11):1542–53.
[19] Ahrenfeldt J, Henriksen U, Jensen TK, Gøbel B, Wiese L, Kather A, et al. Validation of a continuous combined heat and power (CHP) operation of a two-stage boimass gasifier. Energy Fuels 2006;20(6):2672–80.
[20] Hofmann PH, Schweiger A, Fryda L, Panopoulos K, Hohenwarter U, Bentzen J, et al. High temperature electrolyte supported Ni-GDC/YSZ/LSM SOFC operation on two stage Viking gasifier product gas. Power Sources 2007;173(1):357–66.
[21] Elmegaard B, Houbak N. DNA – a general energy system simulation tool. In: Proceeding of SIMS, Trondheim, Norway; 2005.
[22] Perstrup C. Analysis of power plant installation based on network theory. M.Sc. thesis. Denmark: Technical University of Denmark, Laboratory of Energetics; 1989 [in Danish].
[23] Petersen TF, Houbak N, Elmegaard B. A zero-dimensional model of a 2nd generation planar SOFC with calibrated parameters. Int J Thermodyn 2006;9(4):161–9.
[24] Holtappels P, DeHaart LGJ, Stimming U, Vinke IC, Mogensen M. Reaction of CO/CO2 gas mixtures on Ni-YSZ cermet electrode. Appl Electrochem 1999;29:561–8.
[25] Matsuzaki Y, Yasuda I. Electrochemical oxidation of H2 and CO in a H2–H2O–CO–CO2 system at the interface of a Ni–YSZ cermet electrode and YSZ electrolyte. Electrochem Soc 2000;147(5):1630–5.
[26] Keegan KM, Khaleel M, Chick LA, Recknagle K, Simner SP, Diebler J. Analysis of a planar solid oxide fuel cell based automotive auxiliary power unit; 2002. SAE technical paper series No. 2002-01-0413.
[27] Prentice G. Electrochemical engineering principles. Houston, USA: Prentice Hall International; 1991.
[28] Achenbach E. Three-dimensional and time-dependent simulation of a planar solid oxide fuel cell stack. Power Sources 1994;49(1–3):333–48.
[29] Zhu H, Kee RJ. A general mathematical model for analyzing the performance of fuel-cell membrane-electrode assemblies. Power Sources 2003;117:61–74.
[30] Costamagna P, Selimovic A, Del Borghi M, Agnew G. Electrochemical model of the integrated planar solid oxide fuel cell (IP-SOFC). Chem Eng 2004;102(1):61–9.
[31] Kim JW, Virkar AV. The effect of anode thickness on the performance of anode-supported solid oxide fuel cell (SOFC-VI), PV99-19. In: Proceedings of the sixth international symposium on SOFCs. The Electrochemical Society; 1999. pp. 830–9.
[32] Smith JM, Van Ness HC, Abbott MM. Introduction to chemical engineering thermodynamics. 7th ed. Boston: McGraw-Hill; 2005.
[33] Winnick J. Chemical engineering thermodynamics. New York: John Wiley &Sons; 1997.
[34] Reader GT. The pseudo Stirling cycle – a suitable performance criterion. In: Proceeding of the 13th intersociety energy conversion engineering conference, 3; 1979. pp. 1763–70. San Diego, California, August 20–25.
[35] Incropera FP, DeWitt DP, Bergman TL, Lavine AS. Introduction to heat transfer. 5th ed. Wiley; 2006, ISBN 978-0471457275; 2006.
[36] Institute of Plumbing & Heating Engineering. Safe hot water temperature. Available online: http://www.chipe.org.uk/Global/databyte/safe%hot%water.pdf; July 2012.
[37] Winkler W, Lorenz H. Design studies of mobile applications with SOFC-heat engine models. Power Sources 2002;106(1–2):338–43.
[38] Foley AC. A unique sub 5kW solid oxide fuel cell/heat engine hybrid generator. Pap Am Chem Soc 2004;49(2):789–91.
[39] Zhao Y, Chen J. Modeling and optimization of a typical fuel cell – heat engine hybrid system and its parametric design criteria. Power Sources 2009;186(1):96–103.
[40] Chen X, Lin B, Chen J. General performance characteristics and parametric optimum criteria of a Braysson-based fuel cell hybrid system. Energy Fuels 2009;23(12):6079–84.
[41] Chen X, Pan Y, Chen J. Performance and evaluation of a fuel cell – thermoelectric generator hybrid system. Fuel Cells 2010;10(6):1164–70.
[42] Chen L, Gao S, Zhang H. Performance analysis and multi-objective optimization of an irreversible solid oxide fuel cell-Stirling heat engine hybrid system. Electrochem Sci 2013;8(8):10772–87.

Nomenclature

A: area, m^2
$\boldsymbol{A}_{i,j}$*:* matrix
B: diffusion coefficient
D_{bin}*:* binary diffusion coefficient
D_{cell}*:* cell diameter, m
$\dot{E}$*:* exergy flow rate, kW
E_{FC}*:* electricity from fuel cell, V
E_{Nernst}*:* Nernst ideal reversible voltage, V
F: Faradays constant, C/mol
g^0*:* Standard Gibbs free energy, J/mol
g_f*:* Gibbs free energy, J/mol
h: enthalpy, J/kg
h_f*:* enthalpy of formation, J/mol
I_{comp}*:* purchase cost of component *k*
i_{as}*:* anode limiting current, mA/cm^2
i_d*:* current density, mA/cm^2
L_{cell}*:* cell length, m
$\dot{n}_{H2}$*:* molar reaction rate of H_2, mol/s
P: power, W
p: pressure, bar
p_{H2}*:* partial pressure for H_2, bar
p_{H2O}*:* partial pressure for H_2O, bar
Q: heat, J/s
T: operating temperature, K
t: thickness, m
R: universal gas constant, J/mol K
RV: reversibility factor
U_F*:* fuel utilization factor
V: volume, m^3
V_{an}*:* anode porosity
W: work, W
X_{H2}*:* mass reaction rate of H_2
Y: molar fraction

Greek symbols

ΔE_{act}*:* activation polarization, V
ΔE_{conc}*:* concentration polarization, V
ΔE_{offset}*:* offset polarization, V

ΔE_{ohm}: Ohmic polarization, V
ΔT_{ml}: logarithmic mean temperature difference, K
ε: effectiveness
η_{rev}: reversible efficiency
η_v: voltage efficiency
η_{mec}: mechanical efficiency
η_{pump}: efficiency of pump
σ: conductivity, S/cm
τ_{an}: anode tortuosity, m
υ: specific volume, m^3/kg

Subscript

an: anode
ca: cathode
el: electrolyte
ref: reference

Abbreviations

AP: anode pre-heater
CHP: combined heat and power
CP: cathode air pre-heater
DNA: dynamic network analysis
GAP: gasifier air pre-heater
CB: catalytic burner
LHV: lower heating value
RH: room heater
SG: steam generator
SOFC: solid oxide fuel cell
WH: water heater